1   **Palaeoclimate evolution across the Cretaceous–Palaeogene boundary**

2   **in the Nanxiong Basin (SE China) recorded by red strata and its**

3   **correlation with marine records**

4   Mingming Ma[a,b], Xiuming Liu[a,b,c*], Wenyan Wang[a,b]

5

6   [a]*Institute of Geography, Fujian Normal University, Fuzhou, 350007, China; E-mail:*

7   *xliu@fjnu.edu.cn*

8   [b]*Key Laboratory for Subtropical Mountain Ecology (Funded by the Ministry of Science and*

9   *Technology and Fujian Province), College of Geographical Sciences, Fujian Normal University,*

10   *Fuzhou, 350007, China;*

11   [c]*Department of Environment and Geography, Macquarie University, NSW 2109, Australia.*

12

13   **Abstract:** The climate during the Cretaceous Period represented one of the

14   "greenhouse states" of Earth's history. Significant transformation of climate patterns

15   and a mass extinction event characterised by the disappearance of dinosaurs occurred

16   across Cretaceous–Palaeogene boundary. However, most records of this interval are

17   derived from marine sediments. The continuous and well-exposed red strata of the

18   Nanxiong Basin (SE China) provide ideal material to develop continental records.

19   Considerable   research   into   stratigraphic,   palaeontological,   chronologic,

20   palaeoclimatic, and tectonic aspects has been carried out for the Datang Profile, which

21   is a type section of a non-marine Cretaceous–Palaeogene stratigraphic division in

22   China. For this study, we reviewed previous work and found that: 1) the existing

23   chronological framework of the Datang Profile is flawed; 2) precise palaeoclimatic

24   reconstruction is lacking because of the limitations of sampling resolution (e.g.

25   carbonate samples) and/or the lack of efficient proxies; and 3) comparisons of climate

Climate of the Past
Discussions

Open Access

EGU

26 changes between marine and continental records are lacking. To resolve these

27 problems, detailed field observations and sampling, as well as environmental

28 magnetic and rare earth element (REE) measurements, were carried out. The results

29 show that: 1) more accurate ages of the Datang Profile range from 72 Ma to 62.8 Ma,

30 based on a combination of the most recently published radiometric, palaeontological

31 and palaeomagnetic ages; 2) there is considerable evidence of palaeosol generation,

32 which indicates that the red strata formed in a long-term hot, oxidizing environment

33 that lacked of underwater condition; 3) haematite was the dominant magnetic mineral

34 in the red strata, and the variation trend of magnetic susceptibility was consistent with

35 the oxygen isotope records from deep-sea sediments, which indicates that the

36 pedogenic intensity was controlled by global climate; and 4) the palaeoclimate

37 changes from 72 Ma to 62.8 Ma in the Nanxiong Basin were consistent with global

38 patterns, and can be divided into three stages: a relatively hot and wet stage during

39 72–71.5 Ma, a cool and arid stage during 71.5–66 Ma, and a relatively hot and wet

40 stage again during 66–62.8 Ma with a notable drying and cooling event at 64.7–63.4

41 Ma. Moreover, there are several sub-fluctuations during each stage. This work

42 provides basic information for further palaeoclimate reconstruction with higher

43 resolution and longer time scales for the Cretaceous to Palaeocene in the Nanxiong

44 Basin, and may even help to test ocean–land climate interactions in the future.

45 **Keywords:** Cretaceous–Palaeogene boundary; Nanxiong Basin; Palaeosol;

46 Environmental magnetism; Palaeoclimate evolution

47 **1 Introduction**

48 The Earth existed in a greenhouse state during the Late Cretaceous (Hay, 2011;

49 Friedrich et al., 2012; Wang et al., 2014); palaeoclimate studies show that based on

50   marine records, the seawater surface temperature near the equator reached up to 36℃

51   during the Late Cretaceous (Linnert et al., 2014), and reconstructed CO_2

52   concentrations reach up to 837 ppm across the Cretaceous–Tertiary boundary, as

53   recorded in palaeosol carbonates in NE China (Huang et al., 2013). The correlation

54   between extreme greenhouse climate and high CO_2 concentration across this

55   boundary may provide insights for global warming in the present (Wang et al., 2013b).

56   The palaeotemperature decreased significantly from the Mesozoic Era to the Cenozoic

57   (Zachos et al., 2001; Hay, 2011), and a mass extinction event occurred across the

58   Cretaceous–Palaeogene boundary (Schulte et al., 2010; Renne et al., 2013); climate

59   changes and biological evolution during this interval have therefore become a

60   research hotspot. However, most studies of climate change across the Cretaceous–

61   Palaeogene boundary have been derived from marine records (Huber et al., 1995;

62   Barrera and Savin, 1999; Cramer et al., 2009; Friedrich et al., 2012; Bodin et al.,

63   2015). Terrestrial palaeoclimate records are few, and published comparisons and

64   correlations between marine and terrestrial palaeoclimate records are even fewer

65   (Wang et al., 2013b).

66   There are many basins with Cretaceous continental sediments distributed across

67   China (Li et al., 2013), such as the Songliao Basin (NE China, Wu et al., 2009;

68   Bechtel et al., 2012; Chamberlain et al., 2013; Wang et al., 2013a, b; Wan et al.,

69   2013), the Sichuan Basin (SW China; Li, 1988; Huang et al., 2012; Li et al., 2015),

70   and the Nanxiong Basin (SE China; Zhao et al., 1991, 2002, 2009; Buck et al., 2004;

71   Clyde et al., 2010; Li et al., 2010; Wang et al., 2015), which provide ideal records for

72   investigation of Cretaceous climate change. Among these basins, continuous and

73   well-exposed red strata consisting of mudstone and sandstone are preserved in the

74   Nanxiong Basin, and many fossils have been found in these red strata, such as

75   charophytes, palynomorphs, ostracods, dinosaurs, dinosaur eggs, and mammals

76   (Zhang, 1992; Zhang et al., 2006, 2013; Clyde et al., 2010; Li et al., 2010). Many

77   studies have focused on the Datang Profile, which is also called the CGY–CGD

78   profile by Chinese and Germany scientists (Zhao et al., 1991; Yang et al., 1993; Zhao

79   & Yan, 2000). Studies of this profile have investigated its stratigraphy, palaeontology,

80   geochronology, and palaeoclimatology (Zhao et al., 1991; Zhang, 1992; Zhang et al.,

81   2006, 2013; Clyde et al., 2010; Tong et al., 2013; Wang et al., 2015), because it spans

82   from the Upper Cretaceous to the Lower Palaeocene and is a type section for non-

83   marine Cretaceous–Palaeogene stratigraphic division in China. However, precise

84   reconstruction of the palaeoclimatic evolution of this section and comparison with

85   marine records are still lacking because of the lack of efficient proxies. Moreover,

86   many Cretaceous–Palaeogene records are also lacking from low-latitudes in this part

87   of the word, therefore, it is of great significance to carry out paleoclimate change

88   studies here.

89   Environmental magnetism as a proxy has been widely used in the studies of

90   palaeoclimatic changes in Quaternary loess–palaeosol successions (Evans & Heller,

91   2001; Hao & Guo, 2005; Maher & Possolo, 2013; Maher, 2016), Tertiary red clay

92   successions (Liu et al., 2003; Nie et al., 2008; Zhao et al., 2016), and other older

93   aeolian deposits (Hao et al., 2008; Tao et al., 2011), as well as in studies of lake

94   sediments (Snowball et al., 1999; Fu et al., 2015; Hu et al., 2015), and marine

95   sediments (Larrasoaña et al., 2008; Peters et al., 2010). In this paper, we review

96   previous work (mainly in terms of geochronology and palaeoclimatology) and report

97   some defects in the established chronological framework and palaeoclimatic record.

98   Therefore, the aims of this work are to: 1) establish a new chronological framework

99   for the Datang Profile, 2) reinterpret the environment in which the red strata formed, 3)

100   try to reconstruct the palaeoclimatic changes using magnetic parameters, and 4)

101   compare the terrestrial records with marine records to provide reliable terrestrial

102   records for future investigation of ocean–land climate interactions.

103   **2   Geological background, materials, and methods**

104   **2.1 Geological background**

105   The Nanxiong Basin (25°03′–25°16′N, 114°08′–114°40′E) is a rift basin that

106   developed on pre-Jurassic basement, and is controlled by the Nanxiong Fault (Shu et

107   al., 2004). Most of this basin is located in northern Guangdong Province, SE China

108   (Fig. 1A). The basin is elongated with its axis oriented northeast–southwest (Fig. 1B),

109   and is distributed in an area between the Zhuguang and Qingzhang granites (Shu et al.,

110   2004). The modern mean annual rainfall and temperature are ~1,555 mm and ~19.9℃,

111   respectively (data from China Meteorological Data Service Center). Continuous

112   successions of red fluvial–lacustrine clastics, with a maximum thickness of more than

113   7 km, are preserved in the basin. These successions span the Upper Cretaceous,

114   represented by the dinosaur-bearing Nanxiong Group (Changba, Jiangtou, Yuanpu,

115   Dafeng, Zhutian, and Zhenshui Formations), and the Lower Palaeocene, represented

116   by the mammal-bearing Luofuzhai Group (Shanghu, Nongshan, and Guchengcun

117   Formations) (Zhang et al., 2013). Components of conglomerate and coarse-grained

118   sandstone in the basin are similar to those of adjacent strata; moreover, pebbles found

119   in the basin are relatively coarse, poorly sorted, and sharp-edged, which implies that

120   the sediment source was not far from the basin (Shu et al., 2004), and that erosion was

121   stable though the Late Cretaceous to Early Palaeocene (Yan et al., 2007).

Climate
of the Past
Discussions
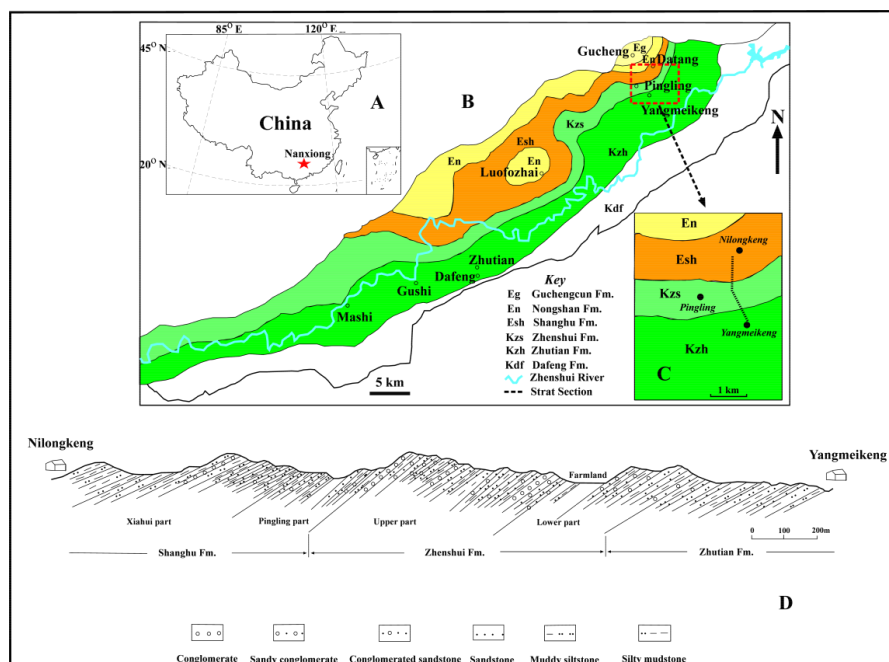
Fig. 1 Sketch map of the Nanxiong Basin: A) location of Nanxiong Basin, B)

stratigraphy of the Nanxiong Basin (from the Dafeng Formation to the Guchengcun

Formation, modified from Li et al., 2010), C) sampling route of the Datang Profile, D)

stratigraphy of the Datang Profile (modified from Zhang et al., 2006)

Several profiles in the basin have been investigated since the 20th century (Zhao

et al., 1991, 2002; Zhang & Li, 2000; Zhang et al., 2006, 2013; Zhang & Li, 2015). Of

these profiles, the Datang Profile (Fig. 1C), with a vertical thickness of ~700 m, was

the most thoroughly investigated because of clear stratigraphic succession and

abundant fossils. The Datang Profile consists of three formations (Fig. 1D, Zhang et

al., 2006); from bottom to top these are the Zhutian Formation (105 m), the Zhenshui

Formation (295.5 m), and the Shanghu Formation (288.3 m), which are described in

detail below (Zhang et al., 2006; Wang, 2012; Zhang, 2016).

135   The Zhutian Formation consists mainly of brown-red, dark purple muddy

136   siltstone, and silty mudstone with fine sandstone interbeds. Large quantities of

137   ostracods and charophytes, and minor amounts of gastropods, conchostracans, and

138   dinosaur footprints have been discovered. Several moderately to fully mature

139   palaeosol layers with calcareous nodules generated in this formation.

140   The Zhenshui Formation is predominantly composed of coarse clastic deposits,

141   represented by grey-purple sandstone and conglomerate with red silty mudstone

142   interbeds. This formation is rich in vertebrate and dinosaur eggs, with minor amounts

143   of ostracods, charophytes, bivalves, and gastropods. A few moderately to fully mature

144   palaeosol layers generated in this formation.

145   The Shanghu Formation is predominantly composed of purple and dark brown

146   muddy siltstone and silty mudstone with numerous calcareous nodules and thin

147   interbeds of sandstone and conglomerate. This formation is rich in microfossils such

148   as ostracods and charophytes, and also contains fossils of mammals, turtles,

149   gastropods, and pollen. A great deal of moderately to fully mature palaeosol layers

150   generated in this formation.

151   **2.2 Materials and methods**

152   Powder samples were collected from the Datang Profile; because of strong

153   weathering of the Zhenshui Formation, the sampling intervals for this formation were

154   larger than those for the other formations. To eliminate the effects of particle size on

155   magnetic parameters, the selected samples were mainly muddy siltstone or silty

156   mudstone. All samples were dried naturally in a laboratory, gently ground to

157   disaggregate the grains, and then packed into small non-magnetic plastic boxes (8 cm^3)

158   before measurement. Magnetic susceptibility (χ) was measured using a Bartington

Climate
of the Past
Discussions

Open Access

EGU

159 MS2-B meter at 470 Hz and then normalised by mass. Anhysteretic remanent

160 magnetisation (ARM) was imparted with a peak AF field of 100 mT and a DC bias

161 field of 0.05 mT using a Molspin alternating field demagnetiser, and then measured

162 with a Molspin Minispin magnetometer. Isothermal remanent magnetisation (IRM)

163 was conducted using a Molspin 1 T pulse magnetiser and measured by employing the

164 Minispin magnetometer. The IRM at 1 T was regarded as saturation IRM (SIRM).

165 Backfield remagnetisation of SIRM was carried out using reverse fields at 10 mT

166 steps, and remanence coercivity (Bcr) was calculated using linear interpolation. High-

167 temperature magnetic susceptibility curves (κ-T curves) were obtained using an Agico

168 KLY-3 Kappabridge with a CS-3 high-temperature furnace.

169 Rare earth element (REE) measurements were completed using an X-SERIES

170 inductively coupled plasma-mass spectrometer (ICP-MS). Before measurement, bulk

171 samples were successively treated with HF and HNO_3 (3:1), $HClO_4$, HNO_3

172 ($HNO_3:H_2O = 1:2$), and ultrapure water.

173 All measurements were conducted at the Key Laboratory for Subtropical

174 Mountain Ecology, Fujian Normal University.

175 **3 Results**

176 **3.1 κ-T curves**

177 High-temperature κ-T curves can be used to identify magnetic phases according

178 to their Curie/Neel temperatures (Tc/T_N) or specific decomposition temperatures

179 during the heating process; for example, the Tc/T_N of magnetite and haematite are

180 ~580℃ (Smith, 1956; Levy et al., 2012) and ~670℃ (Lu & Meng, 2010), respectively.

181 Partial substitution of Fe in magnetite or haematite with Ti or Al will decrease their

Climate
of the Past
Discussions

182 Tc temperatures (Jiang et al., 2012, 2015). Maghemite generated during pedogenic

183 processes is generally unstable during heating, as represented by its transformation to

184 haematite at 300–400℃ (Liu et al., 1999). In addition to being affected by the

185 magnetic mineral type, κ-T curves are also affected by magnetic particle size due to

186 that some fine particles could change their domain state during the heating/colling

187 process (Liu et al., 2005).

188   The κ-T curves of pilot samples from the Datang Profile are similar (Fig. 2);

189 heating curves decrease with increasing temperature from room temperature to

190 ~200℃, which suggests the presence of paramagnetic minerals (Evans & Heller,

191 2003). And then gradually increases from 200℃ to ~500-600℃, which may be

192 related to the unblocking effects of fine magnetic particles (Liu et al., 2005). After

193 this step, a T_N of about 640–660℃ is shown, which indicates the presence of

194 haematite, and the decreased T_N temperatures may be related to partial substitution of

195 Fe elements with Al (Jiang et al., 2013, 2014). Most heating and cooling curves are

196 nearly reversible, which indicates that no new magnetic minerals are generated during

197 the heating process; therefore, the haematite is original in the samples.

198

Climate
of the Past

Open Access

EGU

Discussions
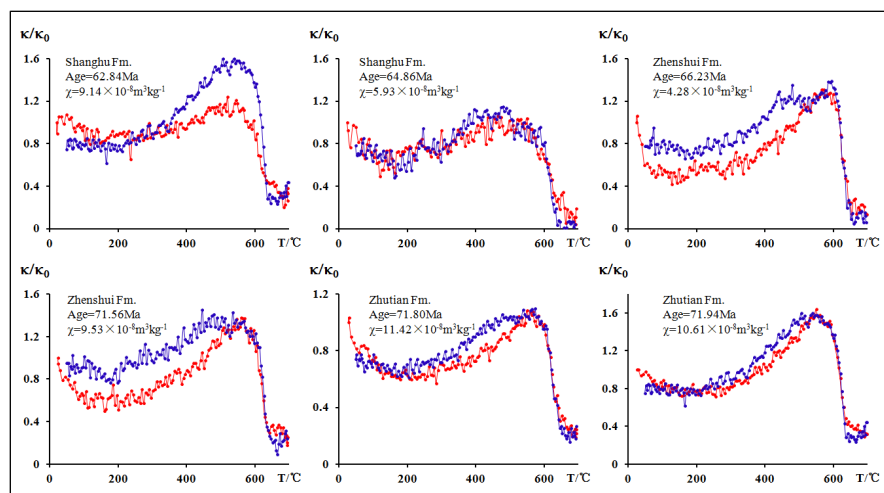
199   **Fig. 2** The κ-T curves of pilot samples from the Datang Profile (red lines represent

200   heating curves, whereas blue lines indicate cooling curves)

201   **3.2 χ, SIRM, HIRM, and B_{cr}**

202   The χ values are controlled by the types, concentrations, and particle sizes of

203   magnetic minerals in the samples; all ferromagnetic, ferrimagnetic, antiferromagnetic,

204   and paramagnetic minerals have effects on χ. In contrast, SIRM, HIRM, and B_{cr} are

205   not affected by paramagnetic minerals or superparamagnetic particles. Therefore,

206   χ and SIRM can be used to indicate the concentration of magnetic minerals in cases

207   where one magnetic mineral is dominant. HIRM can be used to indicate the

208   concentration of hard magnetic minerals such as haematite. The value of B_{cr} can be

209   used to indicate the ratio of hard to soft magnetic minerals (Thompson & Oldfield,

210   1986; Evans & Heller, 2003). As shown in Fig. 3, the values of χ, SIRM, and HIRM

211   are low: χ varies from 1.67 to 19.14 $\times 10^{-8}$ m^3 kg^{-1} with an average value of 7.25 $\times$

212   10^{-8} m^3 kg^{-1}; SIRM varies from 55.27 to 626.26 $\times 10^{-5}$ Am^2 kg^{-1} with an average

213   value of 212.36 $\times 10^{-5}$ Am^2 kg^{-1}; HIRM varies from 24.42 to 341.87 $\times 10^{-5}$ Am^2 kg^{-1}

214   with an average value of 124.11 $\times 10^{-5}$ Am^2 kg^{-1}. In addition, the variation trends of

215   these three parameters are similar: high with clear fluctuations in the Zhutian

216   Formation, a sharply decrease from the Zhutian Formation to the Zhenshui Formation,

217   low values with numerous fluctuations in the Zhenshui Formation, an increase in the

218   Pingling Part of the Shanghu Formation, and an overall decease again with significant

219   variations in the Xiahui Part of the Shanghu Formation. The B_{cr} values vary from 300

220   to 600 mT with an average value of 430 mT, which indicate the dominant role of hard

221   magnetic minerals.

Climate
of the Past
Discussions

222   In addition to haematite, there were significant amounts of paramagnetic

223   minerals in the samples, as shown in κ-T curves (Fig. 2); the presence of

224   paramagnetic minerals may affect χ when the overall value of χ is low. However,

225   SIRM and HIRM are not affected by paramagnetic minerals, and their variation trends

226   are similar to those of χ, which suggests that the variations of χ, SIRM, and HIRM

227   are mainly controlled by the concentration of haematite (Thompson & Oldfield, 1986).
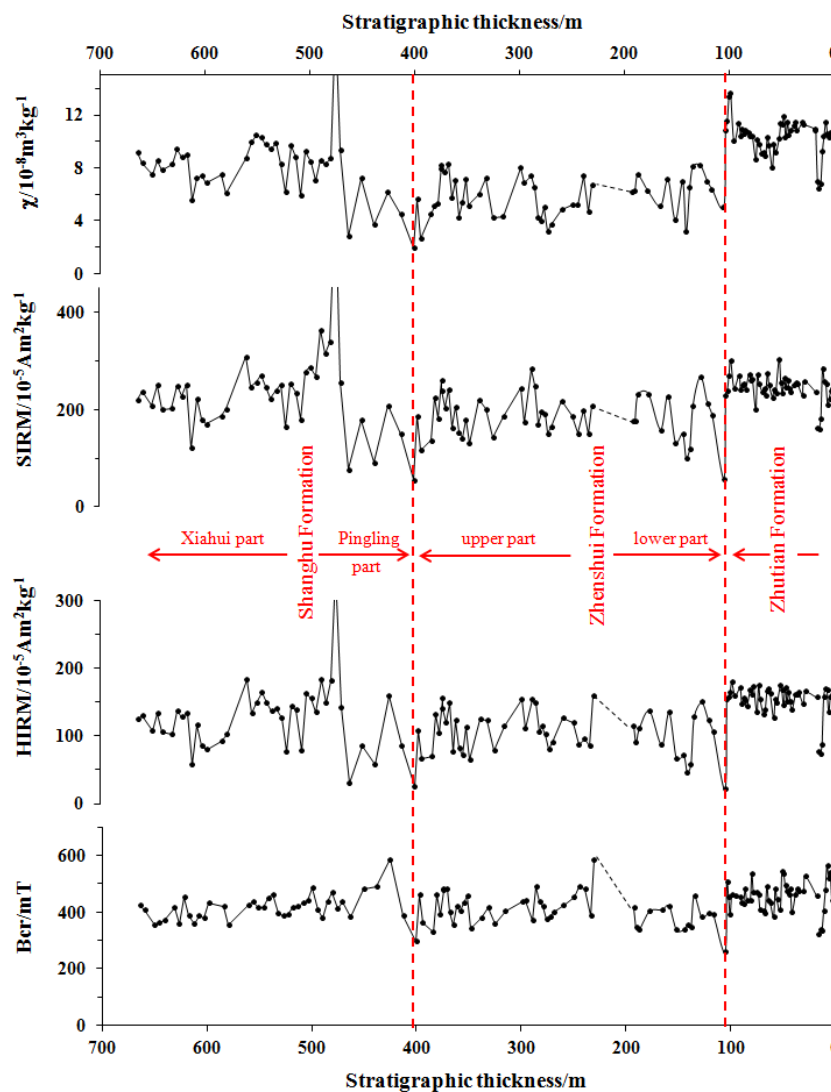

228

229   **Fig. 3** Magnetic parameter variations of the Datang Profile; X axis indicates the

230   stratigraphic thickness from the Zhutian Formation to the Shanghu Formation.

231   **3.3 REEs**

232   There are a variety of distribution patterns of REEs in different types of

233   sediments because of their diverse origins and sources, and the evolution of the

234   palaeoenvironment. Therefore, REEs can be used as efficient tracer elements (Shunso

235   et al., 2010; Fagel et al., 2014). The ΣREE values of the Datang Profile samples vary

236   from 153.71 to 210.18 μg/g, with an average value of 183.28 μg/g. The REE

237   distribution patterns of the pilot samples nearly overlap (Fig. 3); these patterns are

238   characterised by a negative slope, moderate enrichment of LREEs, and a relatively

239   flat HREE pattern, as well as by a prominent negative Eu anomaly, which suggests

240   that the provenance of the red strata remained stable (Yan et al. 2007). These patterns

241   are consistent with those of eight samples from the Zhuguang and Qingzhang granites

242   (Shu et al., 2004), which indicates that they are closely related. However, the Eu

243   anomaly of the granites is more significant than those of the red strata, which is likely

244   related to post-depositional chemical weathering or mixing with other Cambrian–

245   Jurassic sediments (Shu et al., 2004).
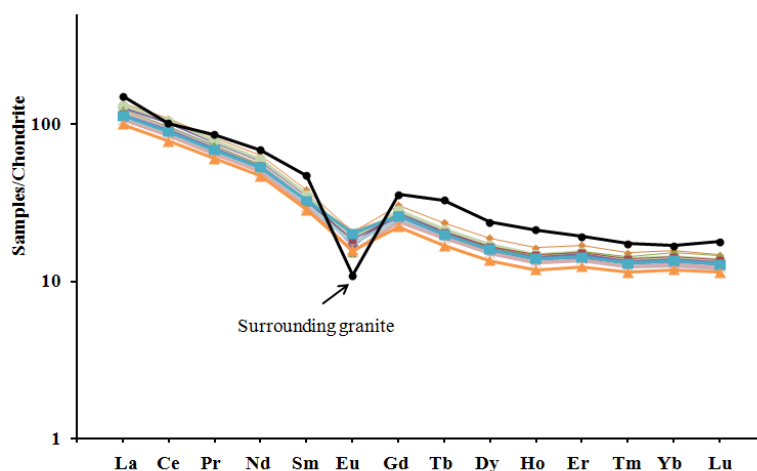
Fig. 4 REE distribution patterns (normalised by chondrite) of pilot samples from the

Datang Profile and samples of the surrounding granite (average values of eight

samples, Shu et al., 2004)

**4 Discussion**

4.1 Chronological framework of the Datang Profile

A great deal of geochronology research, including palaeomagnetic, isotopic, and

palaeontological studies, has been carried out on the Datang Profile (Zhao et al., 1991;

Zhang et al., 2006; Clyde et al., 2010; Li et al., 2010; Tong et al., 2013). The most

significant event recorded in this profile is the extinction of the non-avian dinosaurs

and the subsequent evolutionary radiation of mammals, which indicate the end of the

Cretaceous and the beginning of the Palaeogene (Zhao et al., 1991; Zhang et al., 2006;

Clyde et al., 2010). Based on the palaeontological data and two basalt K–Ar ages

(67.04 ± 2.34, 67.37 ± 1.49 Ma) from the top of the Yuanpu Formation (which

262   corresponds to the Zhutian Formation in this paper), Zhao et al. (1991) suggested that

263   the palaeomagnetic age of the Datang Profile is between 27R and 31R (Fig. 5A).

264   However, Russell et al. (1993) challenged this chronology because of the wide

265   variation of sedimentation rate, which varied by more than an order of magnitude

266   during each chron, proposed an alternative (Fig. 5B), and suggested that several

267   millions of years of deposition was absent from the lowermost part of Palaeocene

268   record. However, there are some fundamental flaws in Russell et al.'s age model. First,

269   a lack of exact ages for palaeomagnetic chron identification made the age model

270   inconclusive. Secondly, based on field observations, no hiatus occurred between the

271   Shanghu Formation and the Zhenshui Formation (Ye et al., 2000; Zhang et al., 2006).

272   Thirdly, it is reasonable to assume that the sedimentary rate differed during different

273   chrons in the Nanxiong Basin, as a continental basin (Ye et al., 2000). Moreover, two

274   U–Pb ages (59.76 ± 0.78, 60.76 ± 0.90 Ma) of a tephra layer from the middle part of

275   the Nongshan Formation, above the Shanghu Formation, were recently obtained

276   (Tong et al., 2013), and confirm that the age model of Russell et al. was incorrect. To

277   further clarify the palaeomagnetism framework of the Datang Profile, Clyde et al.

278   (2010) collected samples from the uppermost 465 m of the Datang Profile (i.e. the

279   lower part of Zhenshui Formation and Shanghu Formation) and the DT05 profile

280   (Nongshan Formation and the lower part of Guchengcun Formation), and combined

281   the results with palaeontological data and δ^{13}C and δ^{18}O isotopic composition data

282   from palaeosol carbonates. The results show that the upper 465 m of the Datang

283   Profile has five well-defined polarity zones (30N, 29R, 29N, 28R, and 28N), whereas

284   the DT05 section is characterised by a single long, reversed-polarity zone (26R),

285   which has been confirmed by the U–Pb ages of the tephra layer from the Nongshan

286   Formation (Tong et al., 2013), and suggests that this chronological work is reasonable.

287   However, the ages of the Zhutian Formation to the upper part of Zhenshui Formation

288   remain unclear.
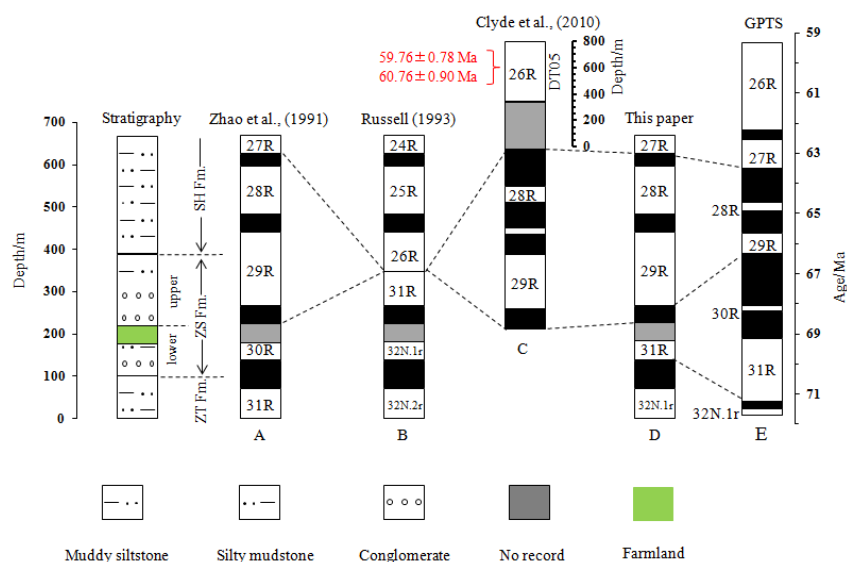
289

290   **Fig. 5** Palaeomagnetic chronology framework of Datang Profile, A) Zhao et al., 1991;

291   B) Russell et al., 1993; C) Clyde et al., 2010; D) this paper; E) Magnetic polarity time

292   scale (Gradstein et al., 2012).

293   The age of the Zhutian Formation to the upper part of the Zhenshui Formation in

294   Zhao's model is controversial; the basalts whose age was used for palaeomagnetic

295   chron identification were actually intrusive rocks that formed after the Zhutian

296   Formation was deposited, and therefore cannot be regarded as the top age of the

297   Zhutian Formation. Thus, the top age of the Zhutian Formation should be older than

298   67.4 Ma (Zhang & Li, 2000), and it was confirmed with biostratigraphic data

299   (*Tenuestheria*) that the Zhenshui Formation correlates with Maastrichtian formations,

300   whereas the Zhutian Formation correlates with lower Santonian–Campanian

301   formations (Li et al., 2010). Therefore, it was incorrect to use 67.4 Ma as the top age

Climate
of the Past

Discussions

Open Access

EGU

302   of the Zhutian Formation in Zhao's model. The Zhenshui Formation is predominantly

303   composed of coarse clastic deposits, and the top 45.2 m of the lower part is covered in

304   farmland (Fig. 1D and Fig. 5); therefore, it is not possible to obtain samples for

305   palaeomagnetic analysis, which likely led to the absence of two short time chrons—

306   30R (0.173 Ma, Gradstein et al., 2012) and 31N (0.9 Ma, Gradstein et al., 2012)—

307   from the palaeomagnetic results. Therefore, a new alternative can be proposed, as

308   shown in Fig. 5D: 30R, 31N, and 31R in Zhao's model are modified to 31R, 32N.1n,

309   and 32N.1r. The calculated boundary age of the Zhenshui and Zhutian Formations is

310   ~71.5 Ma according to the new age model, which is consistent with the

311   biostratigraphic data (Li et al., 2010). According to the chronological framework

312   obtained above, the bottom and top ages of the Datang Profile can be calculated using

313   linear extrapolation as 72 Ma and 62.8 Ma, respectively.

314   **4.2 Sedimentary environment analysis**

315   Many aquatic fossils, such as ostracods and charophytes, were found in the red

316   strata, and there are many coarse sandstone and conglomerate layers; therefore, the

317   sediments were interpreted as fluvial or lacustrine facies in previous studies (Zhang et

318   al., 2006; Clyde et al., 2010; Wang et al., 2015). In greater detail, the Zhutian

319   Formation was regarded as floodplain and shallow lake deposits, the Zhenshui

320   Formation was interpreted as fluvial deltaic deposits, and the Shanghu Formation was

321   regarded as shallow lake deposits (Wang, 2012). However, there are dozens of

322   calcareous nodule layers (Fig. 6A and 6B), generated by pedogenic processes,

323   distributed in muddy sandstone and sandy mudstone layers (Clyde et al., 2010; Wang,

324   2012), especially in the Shanghu and Zhutian Formations. In addition to calcareous

325   nodules, other evidence for palaeosol formation was found, such as wormhole

326   remains (Fig. 6C and 6D), root traces (Fig. 6E) and obvious rhizoliths (Fig. 6F).

327   Moreover, many mud-cracks are observed in the Datang Profile (Figs. 4G and 4H).

328   Mud-cracks mainly form under alternating dry–wet environments, which have

329   traditionally been regarded as an indicator of arid or seasonally arid environments.

330   Environmental magnetic results (Figs. 2 and 3) show that haematite is the dominant

331   magnetic minerals in the red strata. Haematite is an iron oxide that mainly forms and

332   is preserved in oxidising environments, and will be dissolved or transformed under

333   excessively wet and reducing conditions. The widely distributed haematite and

334   palaeosols in the Datang Profile suggest that the sediments were exposed in a

335   relatively arid and oxidising environment.
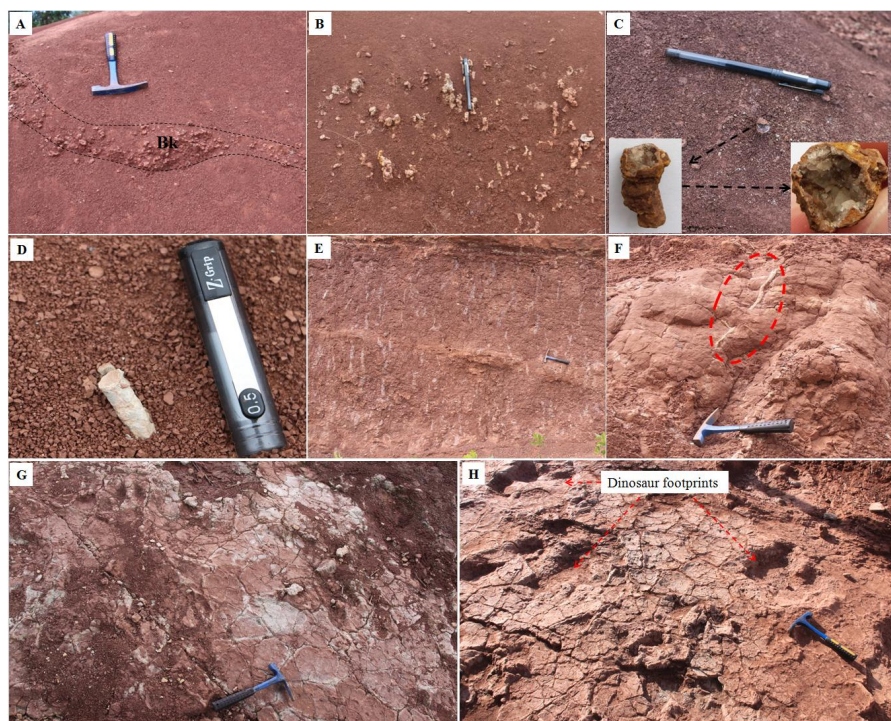
336

337   **Fig. 6** Evidence of palaeosols in the Datang Profile: calcareous nodule layers

338   generated during pedogenic processes (A and B), wormhole remains filled with

339   calcite (C) and grey mudstone (D), root traces (E) and obvious rhizolith (F), as well as

340   mud-cracks (G and F).

341   The climate during the Cretaceous represented one of the "greenhouse states" of

342   Earth history; the maximum CO_2 concentration was nearly 10 times higher and the

343   temperature 3–10℃ higher than those prior to the Industrial Revolution (Huber et al.,

344   2002; Wilson et al., 2002; Retallack, 2009). Although the CO_2 concentration

345   decreased in the Late Cretaceous, it was still higher than today (Wang et al., 2014,

346   and the references therein). The Nanxiong Basin was belonged to a hot and arid belt

347   according to the palaeoclimate classification of Chumakov et al. (2004). Clumped

348   isotope analysis of pedogenic carbonates has shown that the palaeotemperature could

349   reach up to 27.3–38.2℃, with an average value of 34℃ (Zhang, 2016), which

350   suggests that the temperature during the Late Cretaceous to Early Palaeocene was

351   much higher than that of the present in this area. In addition, the $CaCO_3$ contents are

352   10–20% (wt, Yang et al., 2007) in the red strata, and there are many pedogenic

353   carbonate layers in the sandy mudstone and muddy sandstone, which suggest that the

354   leaching process was weak and that rainfall was moderate (Retallack, 1999, 2005;

355   Yan et al., 2007). TOC concentration is very low (0.027–0.258 wt%, Yan et al., 2007),

356   which is likely related to the sparse vegetation coverage or oxidising conditions

357   unfavourable for TOC preservation. Therefore, all geochemical parameters indicate

358   that the overall climate during the Late Cretaceous to Early Palaeocene in the

359   Nanxiong Basin was tropical (semi-) arid.

360   Therefore, the depositional processes of red strata in the Nanxiong Basin under

361   (semi-) arid climate conditions can be inferred as follows. Weathered materials were

362   transported from the surrounding area by runoff caused by rainfall and were then

Climate
of the Past
Discussions

363   deposited in the basin. During the interval with greater rainfall, temporary rivers or

364   lakes appeared in the basin and provided a habitat for the low-level aquatic organisms

365   such as ostracods and charophytes, and left abundant fossils of these organisms in the

366   strata. However, the rivers or lakes could not persist for long in a hot, (semi-) arid

367   climate; after the weathered materials were deposited in the basin, these temporary

368   rivers and lakes disappeared because of strong evaporation, and the sediments were

369   then exposed to an oxidising environment. Haematite was thus generated, and the

370   organic matter rapidly decomposed, which led to very low TOC values (Yan et al.,

371   2007). Pedogenic processes then developed, and moderately to fully mature soils with

372   diagnostic characters such as Bk horizons, wormholes and root traces formed in sandy

373   mudstone and muddy sandstone layers. No typical palaeosols were found in the

374   coarse sandstone or conglomerate layers in the Zhenshui Formation because of the

375   lack of essential conditions for soil formation, but many root traces were preserved

376   (Figs. 6E and 6F), which can be called "weakly developed soils".

377   **4.3 Comparison between χ and $\delta^{18}O$, and the corresponding mechanism**

378   At present, most high-resolution records of palaeoclimate changes during the

379   Late Cretaceous to Early Palaeogene were derived from marine sediments, with few

380   from continental sediments, which has limited comparison between marine records

381   and continental records and even the study of the dynamic mechanism of

382   palaeoclimate evolution (Wang et al., 2013b). The $\delta^{18}O$ values of benthic foraminifera

383   in marine sediments faithfully recorded global palaeotemperature changes over the

384   past 200 Ma (Zachos et al., 2001; Friedrich et al., 2012; Bodin et al., 2015), which has

385   provided a high-resolution reference for the study of continental records (Fig. 7A). As

386   shown in Fig. 7, there is a significant negative correlation between χ and $\delta^{18}O$ for the

387   Pacific and South Atlantic (Friedrich et al., 2012) from 72 Ma to 62.8 Ma: high (low)

388   χ values correlate with low (high) $\delta^{18}O$ values, which suggest that χ values likely

389   recorded the global palaeoclimate evolution.
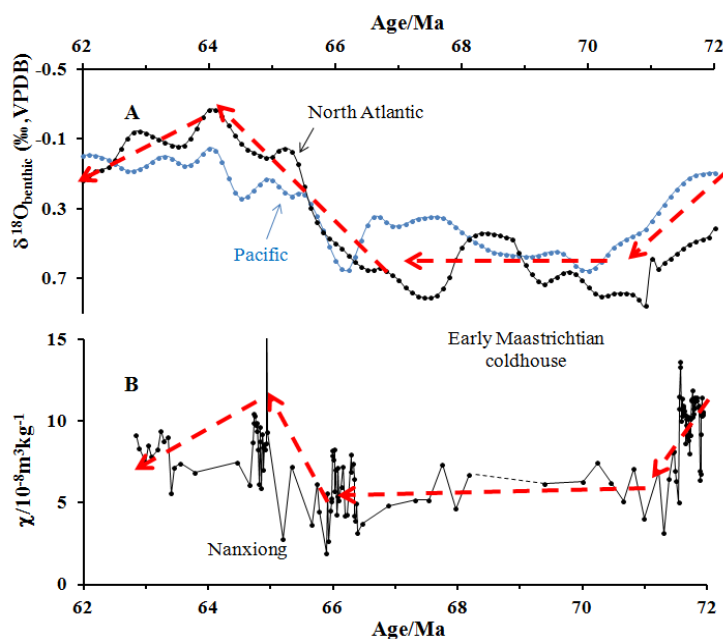
391   **Fig. 7** Correlations between $\delta^{18}O$ from Pacific and North Atlantic records (A) and

392   χ from the Datang Profile (B) from 72 Ma to 62.8 Ma; higher $\delta^{18}O$ values correlate

393   with lower χ values

394   The parameter χ has been widely applied in Chinese Quaternary loess–palaeosol

395   and Tertiary red clay sequences as an efficient palaeoclimatic indicator, and correlates

396   well with the $\delta^{18}O$ values of marine records (Liu, 1985; Nie et al., 2008). Multiple

397   glacial–interglacial cycles occurred during the Quaternary, and the climate during

398   interglacial periods was warmer and more humid than that of glacial periods, which

399   led to the formation of palaeosols. Palaeosols are magnetically enhanced because of

Climate
of the Past

Open Access

Discussions

EGU

400   in-situ pedogenic formation of magnetite and maghemite under elevated temperature

401   and rainfall conditions, which lead to higher χ values in palaeosol layers than in loess

402   layers in the Chinese Loess Plateau (CLP, Zhou et al., 1990; Liu et al., 1992; Maher et

403   al., 1994; Chen et al., 2005; Hao & Guo, 2005). The climate was warmer and more

404   humid during the Tertiary than in Quaternary interglacial periods, according to red

405   clay records (Ding et al., 1999, 2001), but most χ values of red clays were lower than

406   those of Quaternary palaeosols and even lower than those of loess layers (Nie et al.,

407   2008), which indicates that the pedogenic hypothesis cannot be simply applied in red

408   clay layers. The dominant magnetic minerals in loess are original magnetite and

409   haematite, with minor amounts of pedogenic maghemite. In contrast, in palaeosol

410   layers, the dominant magnetic minerals are pedogenic maghemite and magnetite, with

411   minor amounts of magnetite, and in red clay layers, the dominant magnetic minerals

412   are pedogenic haematite with minor pedogenic maghemite (Xie, 2008). As mentioned

413   above, the climate when the red clay layers formed was warmer and more humid, and

414   pedogenesis was stronger; consequently, a large amount of ultrafine strongly

415   magnetic minerals such as maghemite and magnetite formed (Nie et al., 2007, 2014,

416   2016). Previous studies have shown that low-temperature oxidation (LTO) of

417   magnetite is a common process during weathering (VanVelzen & Dekkers, 1999) that

418   gradually alters magnetite into maghemite (magnemitisation). Moreover, chemical

419   weathering can transform maghemite into haematite (Sidhu, 1988; Torrent et al., 2006;

420   Zhang et al., 2012; Fang et al., 2015; Hu et al., 2015). The magnetic minerals in red

421   clays underwent stronger oxidation than Quaternary loess–palaeosol sequences (Nie

422   et al., 2016), which likely caused most soft magnetic minerals (magnetite and

423   maghemite) to transform into hard magnetic mineral-haematite under LTO and

424   chemical weathering processes, and led to a significant decrease of χ values in red

425   clay. Nonetheless, χ values of red clay can still be used as an efficient palaeoclimatic

426   indicator (Nie et al., 2008; Zhao et al., 2016).

427   Generally, palaeosols, even without burial or original gleisation in deep time,

428   have systematically lower χ, such as observed for Precambrian and Palaeozoic

429   palaeosols (Retallack et al., 2003). Two possible explanations for this finding have

430   been proposed: 1) recrystallisation and metamorphism of magnetite and maghemite

431   (Retallack, 1991), and 2) lower biological productivity of such deeply buried and

432   ancient soils (Schwartzmann and Volk, 1991). However, these two possibilities

433   require further testing of palaeosols with a wider range of geological ages and degrees

434   of burial alteration (Retallack et al., 2003). Despite the low values of χ in many of

435   these deep time palaeosols, many studies have concluded that the magnetic minerals

436   preserved in these soils are pedogenic (Rankey and Farr, 1997; Cogoini et al., 2001;

437   Tramp et al., 2004). Therefore, we propose another possibility to explain the low χ in

438   the Nanxiong red strata. The global climate during the Late Cretaceous to Early

439   Palaeocene was much warmer than that of the Neogene and Quaternary (Friedrich et

440   al., 2012; Bodin et al., 2015). The Chemical Index of Alteration (CIA) values of red

441   strata in the Nanxiong Basin (70–80, Yan et al., 2007) are higher than those of

442   Quaternary loess–palaeosol and Tertiary red clay (61–71, Chen et al., 2001; Xiong et

443   al., 2010), which suggests that the red strata underwent stronger chemical weathering.

444   The climate during the Late Cretaceous to Early Palaeocene in the Nanxiong Basin

445   was hot and (semi-) arid, with a certain amount of rainfall, as represented by the

446   presence of temporary rivers and shallow lakes (or low-lying land) and palaeosols

447   with calcareous nodules (Retallack, 1999, 2005), which favoured the LTO of

448   magnetite and the transformation of maghemite to haematite through chemical

449   weathering, caused haematite to be the main magnetic mineral in the red strata (κ-T

450 curves, Fig. 2) and significantly decreased χ. This process is summarised in Fig. 8.

451 The global climate was unstable from 72 Ma to 62.8 Ma, as represented by multiple

452 cycles of cold/warm changes (Fig. 7A). Higher χ values occurred in warmer periods

453 (lower $\delta^{18}O$ values), which is similar to the correlation between the χ values of

454 Chinese loess–palaeosol/red clay successions and $\delta^{18}O$ (Liu, 1985; Nie et al., 2008).

455 There may be two reasons for the changes in χ : 1) changes of sediment provenance,

456 and 2) palaeoclimatic evolution. REE distribution patterns show that the sediment

457 provenance remained similar in the Datang Profile (Fig. 4), and even across the whole

458 basin (Yan et al., 2007), which indicates that palaeoclimatic evolution was the main

459 reason for changes in χ. There are significantly positive correlations between χ, SIRM,

460 and HIRM (Fig. 3), which suggest that χ was controlled by the concentration of

461 haematite (Fig. 2), whereas haematite was generated through LTO and chemical

462 weathering during pedogenesis. Thus, the relationship between χ and haematite

463 content can be explained by the "pedogenic-plus hypothesis": more haematite formed

464 during warmer and wetter periods with stronger pedogenesis, and caused a higher χ,

465 and opposite conditions yielded lower χ values. The similarity of the χ and $\delta^{18}O$

466 curves suggests that the climate changes in the Nanxiong Basin during 72–62.8 Ma

467 were similar to global trends; therefore, χ can still be used as an efficient indicator for

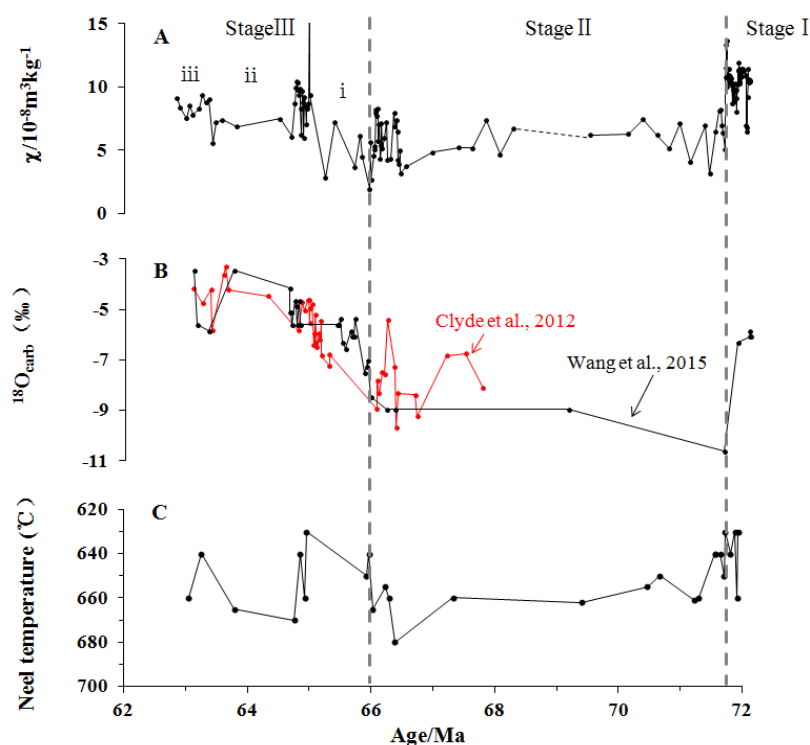468 palaeoclimate changes in this basin.
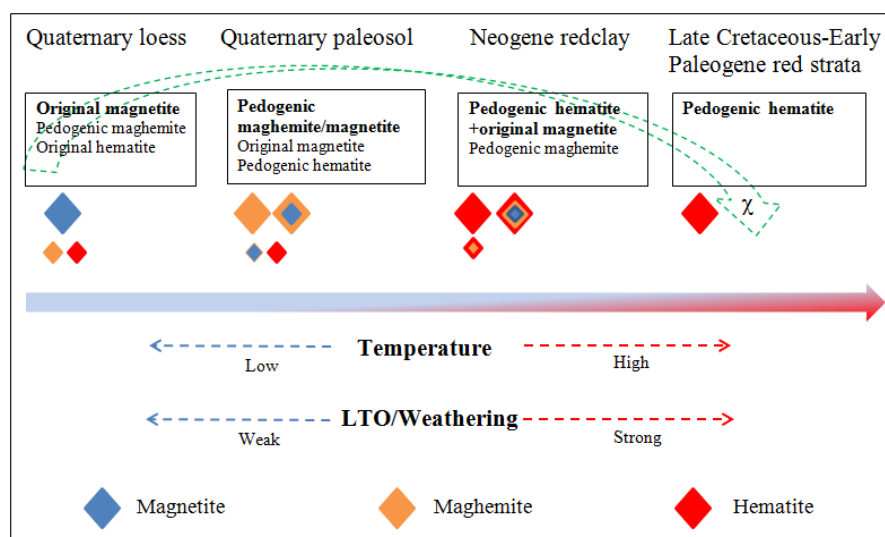
469

470

471   **Fig. 8** Cartoon illustrating the dominant magnetic minerals and χ changes from

472   Quaternary loess–palaeosol (CLP)→Neogene red clay (CLP)→Upper Cretaceous–

473   Lower Palaeogene red strata in Nanxiong Basin along with the increased temperature

474   and LTO/chemical weathering (the size of the symbols means the contribution to

475   χ but not the real size of magnetic particles).

476   **4.4 Palaeoclimatic evolution of the Nanxiong Basin during 72–62.8 Ma**

477   Based on changes of the relative content of clay, the ratio of feldspar to quartz

478   (F/Q) and the $\delta^{18}O$ of pedogenic carbonates, Wang et al. (2012, 2015) divided the

479   palaeoclimatic changes recorded in the Datang Profile into three stages: an arid to

480   semi-arid climate from the Zhutian Formation to the bottom of the Pingling part of the

481   Shanghu Formation, a semi-arid to hot and humid climate from the bottom of the

482   Pingling part to the bottom of the Xiahui part of the Shanghu Formation, and the

483   semi-arid climate of the Xiahui part. Their age model follows the palaeomagnetic

484   framework of Zhao et al. (1991, Fig. 5A). In contrast, Yan et al. (2007) suggested that

485   a long period of extremely dry climate occurred in the Late Cretaceous, and that the

486   climate then became relatively wet in the Early Palaeocene, based on $CaCO_3$ and

487   TOC contents as well as the ratios of Rb/Ti and Cs/Ti. Furthermore, quantitative

488   palaeotemperature data have been successfully determined; for example, clumped

489   isotope analysis of pedogenic carbonates revealed that the palaeotemperature reached

490   up to 27.3–38.2℃ with an average value of 34℃ (Zhang, 2016). Although a

491   considerable amount of work has been conducted on these palaeoclimatic changes, the

492   reconstructed results cannot be compared efficiently with global records. One reason

493   may be the low resolution of quantitative palaeotemperature data due to the

494   limitations of sampling (e.g. pedogenic carbonates), and another may be that the

495   geochronological framework is incorrect (section 4.1). As shown in previous studies,

496   the $\delta^{18}O$ of pedogenic carbonates was found to be an efficient palaeotemperature

497   indicator in terrestrial sediments; greater $\delta^{18}O$ values indicate higher

498   palaeotemperatures (Han et al., 1997; Chamberlain et al., 2012; Gao et al., 2015). In

499   addition, the haematite in the Nanxiong Basin is partially Al-substituted (Fig. 2);

500   indoor examination revealed that there was a negative correlation between T_N and the

501   Al content of Al-substituted haematite (Jiang et al., 2012), and greater Al content in

502   haematite likely indicates stronger pedogenesis. Therefore, we combined these results

503   with the χ curve, $\delta^{18}O$ of pedogenic carbonates (Fig. 9B, Clyde et al., 2010; Wang,

504   2012), and T_N of the pilot samples (Fig. 9C) to reconstruct the climatic evolution of

505   the Nanxiong Basin during 72 to 62.8 Ma.

Climate
of the Past
Discussions

Fig. 9 Combined proxies for palaeoclimatic changes in the Nanxiong Basin from 72 to 62.8 Ma, A) χ curve, B) $\delta^{18}O$ of pedogenic carbonates (Clyde et al., 2010; Wang, 2012), and C) T_N of Al-substituted haematite of pilot samples

Although the palaeoclimate from 72 to 62.8 Ma in the Nanxiong Basin was overall hot and (semi-) arid, it can be divided into three stages, as shown in Fig. 9. For stage I (from 72 to 71.5 Ma, Zhutian Formation), χ and $\delta^{18}O$ values of pedogenic carbonates are relatively high, and T_N is relatively low and varies from 630 to 660℃ with a mean value of 640℃, whereas the $\delta^{18}O$ values of marine sediments are relatively low (Fig. 7); the sediments are mainly composed of muddy siltstone and silty mudstone (shallow lake facies), which indicate a relatively hot and wet climate with stronger pedogenic processes and clear fluctuations, such as the rapid drying and

518   cooling event at ~71.7 Ma, represented by low χ values. In stage II (from 71.5 to 66

519   Ma, Zhenshui Formation), χ decreases sharply at 71.5 Ma and then fluctuates steadily,

520   δ^{18}O values of pedogenic carbonates show a similar trend to χ, T_N is relatively high

521   and varies from 640 to 680℃ with a mean value of 660℃, δ^{18}O of marine sediments

522   first increases and then fluctuates at a high level, and the sediments are mainly

523   composed of coarse sandstone and conglomerate (fluvial delta facies), which indicate

524   a relatively cool and arid climate with weak pedogenesis; these findings are supported

525   by sparse pollen data that show the appearance of the Pinaceae and disappearances of

526   tropical plants in the upper Zhenshui Formation, which indicate a cold climate (Erben

527   et al., 1995). In Stage III (from 66 to 62.8 Ma, Shanghu Formation): χ increases

528   sharply from 66 to ~64.7 Ma, then decreases sharply at 64.7 Ma, and maintains

529   relative low values from 64.7 to ~63.4 Ma, and then returns high values from 63.4 to

530   62.8 Ma; δ^{18}O values of pedogenic carbonates increase rapidly from 66 to ~64.7 Ma

531   and then maintain high values from 64.7 to ~62.8 Ma; T_N of pilot samples and δ^{18}O of

532   marine sediments show opposite trends from χ; the sediments from 66–62.8 Ma are

533   mainly composed of muddy siltstone and silty mudstone (shallow lake facies). In

534   addition, sparse pollen analyses have shown that the climate was temperate–

535   subtropical at the bottom of the Pingling part (~66 to ~65 Ma) (Li, 1989), whereas it

536   was cool and arid in the Xiahui part (Zhang et al., 1981); therefore, the climate

537   changes in this stage can be divided into three sub-stages: in sub-stage i (66–64.7 Ma),

538   the climate quickly became relatively hot and wet from relatively cool and arid

539   conditions; in sub-stage ii (64.7–63.4 Ma), the climate was relatively drying and

540   cooling event represented by low χ values; in sub-stage iii (63.4–62.8 Ma), the

541   climate became relatively hot and wet again.

Climate
of the Past
Discussions

Open Access

EGU

5 Conclusions

542

543   1. Some defects have been identified in the previous palaeomagnetic

544   chronological frameworks because of the lack of reliable control ages for

545   identification of palaeomagnetic chrons. Combined with the most recently published

546   isotopic ages of volcanic ash and biostratigraphic dating, a new chronological

547   framework has been proposed; the results show that the age of the Datang Profile is

548   between 72 to 62.8 Ma.

549   2. Many aquatic fossils, such as ostracods and charophytes, were found in the red

550   strata, and the sediments were interpreted as fluvial or lacustrine facies; however,

551   haematite is the dominant magnetic mineral throughout the profile, and furthermore,

552   palaeosol layers, pedogenic carbonates, wormhole remains, root traces, clear

553   rhizoliths and mud-cracks were found, which indicate that those rivers or lakes, if

554   present, appeared only temporarily in these hot and (semi-) arid environments, such

555   that the sediments were exposed to (semi-) arid and oxidising condition for long

556   periods of time and experienced different degrees of pedogenesis.

557   3. The variations of χ were controlled by the concentration of haematite, which

558   was generated through LTO and chemical weathering during pedogenesis in hot and

559   (semi-) arid environment. Moreover, the stronger the pedogenic processes, the more

560   haematite was generated, and the higher the χ values.

561   4. The χ curve of the Datang Profile is similar to the $\delta^{18}O$ curves of

562   corresponding marine sediments, which suggests that climate changes in the

563   Nanxiong Basin during 72–62.8 Ma were similar to global trends, and can be divided

564   into three stages: 1) a relatively hot and wet climate from 72 to 71.5 Ma with a rapid

565   drying and cooling event at ~71.7 Ma; 2) a relatively cool and arid climate with

566   secondary fluctuations from 71.5 to 66 Ma; and 3) a relatively hot and wet climate

567   again from 66 to 62.8 Ma, which can be divided into 3 sub-stages: i) the climate

568   quickly became hot and wet from 66 to 64.7 Ma, ii) a notable drying and cooling

569   event at 64.7–63.4 Ma, and iii) a relatively hot and wet climate from 63.4 to 62.8 Ma.

570   **Author contribution:** Mingming Ma and Xiuming Liu designed the experiments and

571   Wenyan Wang carried them out. Mingming Ma prepared the manuscript with

572   contributions from all co-authors.

573   **Competing interests:** The authors declare that they have no conflict of interest.

579

580   **References**

581   Barrera, E., Savin, S.M., 1999. Evolution of late Campanian-Maastrichtian marine climates and
582   oceans. In: Barrera, E., Johnson, C. (Eds.), Evolution of the Cretaceous Ocean-Climate
583   System. Geol. Soc. Am. Spec. Pap. 332, 245-282.
584   Bechtel, A., Jia, J., Strobl, S.A.I., Sachsenhofer, R.F., Liu, Z., Gratzer, R., Püttmann, W., 2012.
585   Palaeoenvironmental conditions during deposition of the Upper Cretaceous oil shale
586   sequences in the Songliao Basin (NE China): Implications from geochemical analysis. Org.
587   Geochem. 46, 76-95.
588   Bodin, S., Meissner, P., Janssen, N.M.M., Steuber, T., Mutterlose, J., 2015. Large igneous
589   provinces and organic carbon burial: Controls on global temperature and continental
590   weathering during the Early Cretaceous. Global Planet. Change. 133, 238-253.
591   Buck, B.J., Hanson, A.D., Hengst, R.A., Hu, S.2004. "Tertiary Dinosaurs" in the Nanxiong
592   Basin, Southern China, Are Reworked from the Cretaceous. J. Geol. 112(1), 111-118.
593   Chamberlain, C. P., Mix, H. T., Mulch, A., Hren, M. T., Kent-Corson, M. L., Davis, S. J., Horton,
594   T. W., Graham, S. A., 2012. The Cenozoic climatic and topographic evolution of the western
595   North American Cordillera. Am. J. Sci. 312(2), 213-262.
596   Chamberlain, C.P., Wan, X., Graham, S.A., Carroll, A.R., Doebbert, A.C., Sageman, B.B.,
597   Blisniuk, P., Kent-Corson, M.L., Wang, Z., 2013. Stable isotopic evidence for climate and
598   basin evolution of the Late Cretaceous Songliao basin, China. Palaeogeogr. Palaeoclimatol.
599   Palaeoecol. 385(3), 106-124.
600   Chen, J., An, Z., Liu, L., Ji, J., Yang, J., Chen, Y. 2001. Variations in chemical compositions of
601   the eolian dust in Chinese Loess Plateau over the past 2.5 Ma and chemical weathering in the
602   Asian inland. Sci. China Earth Sci. 44(5), 403-413.

Climate
of the Past
Discussions

603   Chen, T., Xu, H., Xie, Q., Chen, J., Ji, J. Lu, H., 2005. Characteristics and genesis of maghemite
604   in Chinese loess and paleosols: mechanism for magnetic susceptibility enhancement in
605   paleosols, Earth planet. Sci. Lett., 240(3–4), 790–802.
606   Chumakov, N.M. Climatic zones and climate of the Cretaceous period, in: Semikhatov, M.A.,
607   Chumakov, N.M. (Eds.), Climate in the epochs of major biospheric transformations.
608   Transactions of the Geological Institute of the Russian Academy of Sciences, 2004, 105-123.
609   Clyde, W.C., Ting, S., Snell, K.E., Bowen, G.J., Tong, Y., Koch, P.L., :I, Q., Wang, Y., 2010.
610   New Paleomagnetic and Stable-Isotope Results from the Nanxiong Basin, China:
611   Implications for the K/T Boundary and the Timing of Paleocene Mammalian Turnover. J.
612   Geol. 118(2), 131-143.
613   Cogoini, M., Elmore, R.D., Soreghan, G.S., Lewchuk, M.T., 2001. Contrasting rock-magnetic
614   characteristics of two Upper Paleozoic loessite‐paleosol profiles. Phys. Chem. Earth Solid
615   Earth Geod. 26, 905–910.
616   Cramer, B.S., Toggweiler, J.R., Wright, J.D., Katz, M.E., Miller, K.G., 2009. Ocean overturning
617   since the late cretaceous: inferences from a new benthic foraminiferal isotope
618   compilation. Paleoceanography. 24(4), 43-47.
619   Ding, Z.L., Sun, J.M., Yang, S.L., Liu, T.S., 2001. Geochemistry of the pliocene red clay
620   formation in the Chinese Loess Plateau and implications for its origin, source provenance and
621   paleoclimate change. Geochim. Cosmochim. Ac. 65(6), 901-913.
622   Ding, Z.L., Xiong, S.F., Sun, J.M., Yang, S.L., Gu, Z.Y., Liu, T.S., 1999. Pedostratigraphy and
623   paleomagnetism of a ~7.0 Ma eolian loess–red clay sequence at Lingtai, Loess Plateau,
624   north-central China and the implications for paleomonsoon evolution. Palaeogeogr.
625   Palaeoclimatol. Palaeoecol. 152(1–2), 49-66.
626   Erben, H.K., Ashraf, A.R., Böhm, H., Hahn, G., Hambach, U., Krumsiek, K., Stets, J., Thein, J.,
627   Wuster, P., 1995. Die Kreide/Tertiär-Grenze im Nanxiong-Becken (Kontinentalfazies,
628   Südostchina). Erdwissenschaftliche Forschung 32, 245.
629   Evans, M.E., Heller, F., 2001. Magnetism of loess/palaeosol sequences: recent developments.
630   Earth Sci. Rev. 54, 129-144.
631   Evans, M.E., Heller, F., 2003, Environmental magnetismprinciples and applications of
632   environmagnetics. Acdemic Press.
633   Fagel, N., Allan, M., Roux, G.L., Mattielli, N., Piotrowska, N., Sikorski, J., 2014. Deciphering
634   human–climate interactions in an ombrotrophic peat record: REE, ND and Pb isotope
635   signatures of dust supplies over the last 2500 years (Misten bog, Belgium). Geochim.
636   Cosmochim. Ac. 135(7), 288-306.
637   Fang, X., Zan, J., Appel, E., Lu, Y., Song, C., Dai, S., 2015. An Eocene–Miocene continuous rock
638   magnetic record from the sediments in the Xining Basin, NW China: indication for Cenozoic
639   persistent drying driven by global cooling and Tibetan Plateau uplift. Geophys. J. Int. 201(1),
640   78-89.
641   Friedrich, O., Norris, R.D., Erbacher, J. 2012. Evolution of middle to Late Cretaceous oceans—A
642   55 m.y. record of Earth's temperature and carbon cycle. Geology. 40, 107-110.
643   Fu, C., Bloemendal, J., Qiang, X., Hill, M.J., An, Z., 2015. Occurrence of greigite in the Pliocene
644   sediments of Lake Qinghai, China, and its paleoenvironmental and paleomagnetic
645   implications. Geochem. Geophy. Geosy. 16(5), 1293-1306.
646   Gao, Y., Ibarra, D. E., Caves, J. K., Wang, C., Caves, J. K., Chamberlain, C. P., Graham, S. A.,
647   Wu, H., 2015. Mid-latitude terrestrial climate of East Asia linked to global climate in the
648   Late Cretaceous. Geology, 43(4),287-290.
649   Gradstein, F.M., Ogg, J.G., Schmitz, M.D., Ogg, G.M., 2012. The geologic time scale. Elsevier.
650   Han, J., Keppens, E., Liu, T., Paepe, R., Jiang, W., 1997. Stable isotope composition of the
651   carbonate concretion in loess and climate change. Quatern. Int. 37(2), 37-43.
652   Hao, Q. Z., Oldfield, F., Bloemendal, J., Guo, Z. T., 2008. A preliminary study of the magnetic
653   properties of loess and palaeosol samples from the Chinese Loess Plateau spanning the last
654   22 million years. Palaeogeogr. Palaeoclimatol. Palaeoecol. 260(3), 389-404.
655   Hao, Q., Guo, Z., 2005. Spatial variations of magnetic susceptibility of Chinese loess for the last
656   600 kyr: implications for monsoon evolution. J. Geophys. Res.-Solid Earth, 110, B12101,
657   doi:10.1029/2005JB003765.
658   Hay, W.W., 2011. Can humans force a return to a 'Cretaceous' climate? Sediment. Geol. 235,

Climate
of the Past
Discussions

659   5-26.
660   Hu, S., Goddu, S.R., Herb, C., Appel, E., Lleixner, G., Wang, S., Yang, X., Zhu, X., 2015.
661   Climate variability and its magnetic response recorded in a lacustrine sequence in Heqing
662   basin at the SE Tibetan Plateau since 900 ka. Geophys. J. Int. 2015, 201(1), 444-458.
663   Huang, C., Retallack, G.J., Wang, C., Huang, Q., 2013. Paleoatmospheric pCO_2, fluctuations
664   across the Cretaceous–Tertiary boundary recorded from paleosol carbonates in NE china.
665   Palaeogeogr. Palaeoclimatol. Palaeoecol. 385(3), 95-105.
666   Huang, C.M., Retallack, G.J., Wang, C.S., 2012. Early Cretaceous atmospheric pCO_2 levels
667   recorded from pedogenic carbonates. Cretaceous Res. 33, 42-49.
668   Huber, B.T., Hodell, D.A., Hamilton, C.P., 1995. Mid- to Late Cretaceous climate of the southern
669   high latitudes: stable isotopic evidence for minimal equator-to-pole thermal gradients. Geol.
670   Soc. Am. Bull. 107, 392-417.
671   Huber, B.T., Norris, R.D., Macleod, K.G., 2002. Deep-sea paleotemperature record of extreme
672   warmth during the Cretaceous. Geology. 30(2), 123-126.
673   Jiang, Z., Liu, Q., Barrón, V., Torrent, J., Yu, Y., 2012. Magnetic discrimination between Al-
674   substituted hematites synthesized by hydrothermal and thermal dehydration methods and its
675   geological significance. J. Geophys. Res.-Solid Earth, 117 (B2), 119-130.
676   Jiang, Z., Liu, Q., Zhao, X., Jin, C., Liu, C., Li, S., 2015. Thermal magnetic behaviour of Al-
677   substituted haematite mixed with clay minerals and its geological significance. Geophys. J.
678   Int. 200(1), 130-143.
679   Larrasoaña, J.C., Roberts, A.P., Rohling, E.J., 2008. Magnetic susceptibility of eastern
680   Mediterranean marine sediments as a proxy for Saharan dust supply? Mar. Geol. 254(3-4),
681   224-229.
682   Levy, D., Giustetto, R., Hoser, A., 2012. Structure of magnetite (Fe_3O_4) above the Curie
683   temperature: a cation ordering study. Phys. Chem. Miner. 39(2), 169-176.
684   Li, G., Hirano, H., Batten, D.J., Wan, X., 2010, Biostratigraphic significance of spinicaudatans
685   from the Upper Cretaceous Nanxiong Group in Guangdong, South China. Cretaceous Res.
686   31(4), 387-395.
687   Li, J., Wen, X.Y., Huang, C.M., 2015. Lower Cretaceous paleosols and paleoclimate in Sichuan
688   Basin, China. Cretaceous Res. 62, 154-171.
689   Li, M., 1989. Sporo-pollen from Shanghu Formation of Early Paleocene in Nanxiong Basin,
690   Guangdong. Acta Palaeontologica Sinica. 28 (6), 741-750. (in Chinese with English abstract)
691   Li, X., Xu, W., Liu, W., Zhou, Y., Wang, Y., Sun, Y., Liu, L., 2013. Climatic and environmental
692   indications of carbon and oxygen isotopes from the Lower Cretaceous calcrete and lacustrine
693   carbonates in Southeast and Northwest China. Palaeogeogr. Palaeoclimatol. Palaeoecol.
694   385(3), 171-189.
695   Li, Y.W., 1988. The Application of Ostracoda to the Location of the Non-marine Jurassic-
696   Cretaceous Boundary in the Sichuan Basin of China. Developments in Palaeontology &
697   Stratigraphy, 11, 1245-1260.
698   Linnert, C., Robinson, S.A., Lees, J.A., Bown, P.R., Pérez-Rodriguez, I., Petrizzo, M.R., Falzoni,
699   F., Littler, K., Arz, J.A., Russell, E.E., 2014. Evidence for global cooling in the Late
700   Cretaceous. Nat. Commun. 5, 4194.
701   Liu, Q.S., Deng, C.L., Yu, Y.J., Torrent, J., Jackson, M.J., Banerjee, S.K., Zhu, R., 2005.
702   Temperature dependence of magnetic susceptibility in an argon environment: implications
703   for pedogenesis of Chinese loess/palaeosols. Geophys. J. Int. 161, 102-112.
704   Liu, T.S., 1985. Loess and Environment. Beijing: Science Press. 1-481. (in Chinese)
705   Liu, X., Shaw, J., Liu, T., Heller, F., Yuan, B., 1992. Magnetic mineralogy of Chinese loess and
706   its significance, Geophys. J. Int. 108(1), 301-308.
707   Liu, X.M., Hesse, P., Rolph, T., 1999. Origin of maghaemite in Chinese loess deposits: Aeolian or
708   pedogenic? Phys. Earth Planet Inter. 112, 191-201.
709   Liu, X.M., Rolph, T., An, Z., Hesse, P., 2003. Paleoclimatic significance of magnetic properties
710   on the Red Clay underlying the loess and paleosols in China. Palaeogeogr. Palaeoclimatol.
711   Palaeoecol. 199(1-2), 153-166.
712   Lu, H.M., Meng, X.K., 2010. Morin Temperature and Néel Temperature of Hematite Nanocrystals.
713   J. Phys. Chem. C. 114(49), 21291-21295.
714   Maher, B.A., 2016. Palaeoclimatic records of the loess/palaeosol sequences of the Chinese Loess
715   Plateau. Quaternary Sci. Rev. 154, 23-84.

716 Maher, B.A., Possolo, A., 2013. Statistical models for use of palaeosol magnetic properties as
717   proxies of palaeorainfall. Global Planet. Change. 111(12), 280-287.
718 Maher, B.A., Thompson, R., Zhou, L.P., 1994. Spatial and temporal reconstructions of changes in
719   the Asian palaeomonsoon—a new mineral magnetic approach, Earth planet. Sci. Lett. 125,
720   461–471
721 Nie, J., King, J.W., Fang, X., 2007. Enhancement mechanisms of magnetic susceptibility in the
722   Chinese red-clay sequence. Geophys. Res. Lett. 341(19), 255-268.
723 Nie, J., King, J.W., Fang, X., 2008. Link between benthic oxygen isotopes and magnetic
724   susceptibility in the red‐clay sequence on the Chinese Loess Plateau. Geophys. Res. Lett.
725   35(3), 154-175.
726 Nie, J., Song, Y., King, J., 2016. A review of recent advances in red-clay environmental
727   magnetism and paleoclimate history on the Chinese Loess Plateau. Front. Earth Sci. 4: 27 doi:
728   10.3389/feart.2016.00027
729 Nie, J., Zhang, R., Necula, C., Heslop, D., Liu, Q., Gong, L., Banerjee, S., 2014. Late Miocene–
730   early Pleistocene paleoclimate history of the Chinese Loess Plateau revealed by remanence
731   unmixing. Geophys. Res. Lett. 41(6), 2163–2168.
732 Peters, C., Austin, W.E.N., Walden, J., Hibbert, F.D., 2010. Magnetic characterisation and
733   correlation of a Younger Dryas tephra in North Atlantic marine sediments. J. Quaternary Sci.
734   25(3), 339-347.
735 Rankey, E.C., Farr, M.R., 1997. Preserved pedogenic mineral magnetic signature, pedogenesis,
736   and paleoclimate change. Pennsylvanian Roca Shale (Virgilian, Asselian), central Kansas,
737   USA. Sediment. Geol. 114, 11–32.
738 Renne, P.R., Deino, A.L., Hilgen, F.J., Kuiper, K.F., Mark, D.F., Mitchell, W.S., Morgan, L.E.,
739   Mundil, R., Smit, J., 2013. Time Scales of Critical Events Around the Cretaceous-Paleogene
740   Boundary. Science. 339, 684-687.
741 Retallack, G. J., Sheldon, N. D., Cogoini, M., Elmore, R. D., 2003. Magnetic susceptibility of
742   early Paleozoic and Precambrian paleosols. Palaeogeogr. Palaeoclimatol. Palaeoecol. 198(3-
743   4), 373-380.
744 Retallack, G.J, 2009. Greenhouse crises of the past 300 million years. Geol. Soc. Am. Bull. 121(9-
745   10), 1441-1455.
746 Retallack, G.J., 1991. Untangling the e!ects of burial alteration and ancient soil formation. Annu.
747   Rev. Earth Planet. Sci. 19, 183-206.
748 Retallack, G.J., 1999. Depth to pedogenic carbonate horizon as a paleoprecipitation indicator?:
749   Comment and Reply. Geology. 27(12), 41-52.
750 Retallack, G.J., 2005. Pedogenic carbonate proxies for amount and seasonality of precipitation in
751   paleosols. Geology. 33(4), 333-336.
752 Russell, D.A., Russell, D.E., Sweet, A.R., 1993. The end of the dinosaurian era in the Nanxiong
753   Basin. Certebrata Palasiatica, 1993, 31(2): 139-145
754 Schulte, P., Alegret, L., Arenillas, I., Arz, J.A., Barton, P.J., Bown, P.R., Bralower, T.J.,
755   Christeson, G.L., Claeys, P., Cockell, C.S., Collins, G.S., Deutsch, A., Goldin, T.J., Goto, K.,
756   Grajales-Nishimura, J.M., Grieve, R.A.F., Gulick, S.P.S., Johnson, K.R., Kiessling, W.,
757   Koeberl, C., Kring, D.A., Macleod, K.G., Matsui, T., Melosh, J., Montanari, A., Morgan, J.V.,
758   Neal, C.R., Norris, R.D., Pierazzo, E., Ravizza, G., Rebolledo-Vieyra, M., Reimold, W.U.,
759   Robin, E., Salge, T., Speijer, R.P., Sweet, A.R., Urrutia-Fucugauchi, J., Vajda, V., Whalen,
760   M.T., Willumsen, P.S., 2010. Response—Cretaceous Extinctions. Science. 328, 975-976.
761 Schwartzmann, D.W., Volk, T., 1991. Biotic enhancement of weathering and surface temperatures
762   of Earth since the origin of life. Palaeogeogr. Palaeoclimatol. Palaeoecol. 90, 357-371.
763 Shu, L., Deng, P., Wang, B., Tan, Z., Yu, X., Sun, Y., 2004. Lithology, kinematics and
764   geochronology related to Late Mesozoic basin-mountain evolution in the Nanxiong-
765   Zhuguang area, South China. Sci. China Earth Sci. 47 (8), 673-688.
766 Shunso, I., Hua, R., Mihoko, H., Hiroyasu, M., 2010. REE Abundance and REE Minerals in
767   Granitic Rocks in the Nanling Range, Jiangxi Province, Southern China, and Generation of
768   the REE-rich Weathered Crust Deposits. Resour. Geol. 58(4), 355-372.
769 Sidhu, P.S., 1988. Transformation of trace element-substituted maghemite to hematite, Clay.
770   Miner. 36(1), 31-38.
771 Smith, D.O., 1956. Magnetization of a Magnetite Single Crystal Near the Curie Point. Phys. Rev.
772   102(4), 959-963.

Snowball, I., Sandgren, P., Petterson, G., 1999. The mineral magnetic properties of an annually laminated Holocene lake-sediment sequence in northern Sweden. Holocene. 9(3), 353-362.

Thompson, R., Oldfield, F., 1986. Environmental Magnetism. London: Allen & Unwin, 1-228.

Tong, Y., Li, Q., Wang, Y.Q., 2013. An Introduction to recent advance in the study of the continental Early Paleogene stages in China. Journal of Stratigraphy. 37(4), 428-440. (In Chinese with English abstract)

Torrent, J., Barrón, V. Liu, Q.S., 2006. Magnetic enhancement is linked to and precedes hematite formation in aerobic soils. Geophys. Res. Lett. 33, L02402, doi:10.1029/2005GL024818.

Tramp, K.L., Soreghan, G.S., Elmore, R.D., 2004. Paleoclimatic inferences from paleopedology and magnetism of the Permian Maroon Formation loessite, Colorado, USA. Geol. Soc. Am. Bull. 116, 671.

Van Velzen, A.J., Dekkers, M.J., 1999. Low-temperature oxidation of magnetite in loess-paleosol sequences: a correction of rock magnetic parameters, Stud. Geophys. Geod. 43, 357–375.

Wan, X., Zhao, J., Scott, R.W., Wang, P., Feng, Z., Huang, Q., Xi, D., 2013. Late Cretaceous stratigraphy, Songliao Basin, NE China: SK1 cores. Palaeogeogr. Palaeoclimatol. Palaeoecol. 385(3), 31-43.

Wang, C., Feng, Z., Zhang, L., Huang, Y., Cao, K., Wang, P., Zhao, B., 2013a. Cretaceous paleogeography and paleoclimate and the setting of SKI borehole sites in Songliao Basin, northeast China. Palaeogeogr. Palaeoclimatol. Palaeoecol. 385(5), 17-30.

Wang, C., Scott, R.W., Wan,X., Graham, S.A., Huang, Y., Wang, P., Wu, H., Dean, W.E., Zhang, L., 2013b. Late Cretaceous climate changes recorded in Eastern Asian lacustrine deposits and North American Epieric sea strata. Earth-Sci. Rev. 126, 275-299.

Wang, Y., 2012. Paleoclimate changes of thr Late Cretaceous-Late Paleocene in the Nanxiong Basin, South China. Nanjing University, (in Chinese with English abstract)

Wang, Y., Huang, C., Sun, B., Quan, C., Wu, J., Lin, Z., 2014. Paleo-CO_2 variation trends and the Cretaceous greenhouse climate. Earth-Sci. Rev. 129, 136-147.

Wang, Y., Li, X., Zhou, Y., Liu, L., 2015. Paleoclimate indication of Terrigenous clastic rock's component during the Late Cretaceous-Early Pa;Eocene in the Nanxiong Basin. Acta Sedimentologica Sinica. 33(1), 116-123. (In Chinese with English abstract)

Wilson, P.A., Norris, R.D., Cooper, M.J., 2002. Testing the Cretaceous greenhouse hypothesis using glassy foraminiferal calcite from the core of the Turonian tropics on Demerara Rise. Geology. 30(7), 607-610.

Wu, H., Zhang, S., Jiang, G., Huang, Q., 2009. The floating astronomical time scale for the terrestrial Late Cretaceous Qingshankou Formation from the Songliao Basin of Northeast China and its stratigraphic and paleoclimate implications. Earth Planet. Sc. Lett. 278(3-4), 308-323.

Xie, Q., 2008. Nanominerals of the loess-red clay sequences in Chinese Loess Plateau. Hefei University of Technology. (in Chinese with English abstract)

Xiong, S., Ding, Z., Zhu, Y., Zhou, R., Lu, H., 2010. A ~6 Ma chemical weathering history, the grain size dependence of chemical weathering intensity, and its implications for provenance change of the Chinese loess–red clay deposit. Quaternary Sci. Rev. 29(15), 1911-1922.

Yan, Y., Xia, B., Lin, G., Cui, X., Hu, X., Yan, P., Zhang, F., Geochemistry of the sedimentary rocks from the Nanxiong Basin, South China and implications for provenance, paleoenvironment and paleoclimate at the K/T boundary. Sediment. Geol. 197(1-2), 127-140.

Yang, W., Chen, N., Ni, S., Nan, J., Wu, M., Jiang, J., Ye, J., Feng, X., Ran, Y., 1993. Carbon and Oxygen Isotopic Compositions of the Carbonate Rocks and the Dinosaur Eggshells in the Cretaceous Red Beds and Their Implication for Paleoenvironment. Chinese Sci. Bull. 38(23), 1985-1989.

Ye, J., 2000. Discussion on the problems of the K/T Boundary in the Nanxiong Basin. Certebrata Palasiatica, 38(1), 1-9.

Zachos, J., Pagani, M., Sloan, L., Thomas, E., Billups, K., 2001. Trends, Rhythms, and Aberrations in Global Climate 65 Ma to Present. Science. 292(5517), 686-693.

Zhang X, Li G. Discussion on geological age of the Pingling Member of Shanghu Formation in the Nanxiong Basin,Guangdong Province. Journal of Stratigraphy, 2015,39 (1): 74-80. (In Chinese with English abstract)

Zhang, L., 2016. Paleoclimatic evolution and mechanism of the mass extinction during the K-Pg boundary: Evidences from several terrestrial basins in East China. China University of

830   Geosciences (Beijing). (in Chinese with English abstract)

831 Zhang, Q., 1981, Paleocene sporopollen assemblages in the Nanxiong Basin Guangdong Province.
832   In: Bull. Yichang Inst. Geol. M. R., Chinese Acad. Geol. Sci. Sp. Iss. S. P. 106-117. (in
833   Chinese with English abstract)

834 Zhang, T., Guo, Z.T., Wu, H.B., Ge, J., Zhou, X., Wu, C., Zeng, F., 2011. Thick Miocene eolian
835   deposits on the Huajialing Mountains: The geomorphic evolution of the western Loess
836   Plateau. Sci. China Earth Sci. 54(2), 241-248.

837 Zhang, W., Erwin, A., Fang, X., Yan, M., Song, C., Cao, L., 2012. Paleoclimatic implications of
838   magnetic susceptibility in Late Pliocene–Quaternary sediments from deep drilling core SG-1
839   in the western Qaidam Basin (NE Tibetan Plateau). J. Geophys. Res. 117(B6), 6101.
840   doi:10.1029/2011JB008949.

841 Zhang, X., 1992. A study on Ostracod fauna of Shanghu Formation and Cretaceous-Tertiary
842   Boundary in Nanxiong Basin, Guangdong. Acta Micropalaeontologica Sinica. 6, 678-702.
843   (In Chinese with English abstract)

844 Zhang, X., Li, S., 2000. New progress in stratigraphic study of the western area of Nanxiong
845   Basin. Guangdong Geology. 15(1), 9-18. (In Chinese with English abstract)

846 Zhang, X., Lin, J., Li, G., Lin, Q., 2006. Non-marine Cretaceous-Paleogene boundary section at
847   Datang, Nanxiong, northern Guangdong. Journal of Stratigraphy. 30(4), 327-340. (In Chinese
848   with English abstract)

849 Zhang, X., Zhang, X., Hou, M., Li, G., Li, H., 2013. Lithostratigraphic subdivision of red beds in
850   Nanxiong Basin, Guangdong, China. Journal of Stratigraphy. 37(4), 441-451. (In Chinese
851   with English abstract)

852 Zhao, G., Han, Y., Liu, X., Chang, L., Lü, B., Chen, Q., Guo, X., Yan, J., Yan, J., 2016. Can the
853   magnetic susceptibility record of Chinese Red Clay sequence be used for palaeomonsoon
854   reconstructions?. Geophys. J. Int. 204(3), 1421-1429.

855 Zhao, Z., Mao, X., Chai, Z., Yang, G., Zhang, F., Yan, Z., 2009. Geochemical environmental
856   changes and dinosaur extinction during the Cretaceous-Paleogene (K/T) transition in the
857   Nanxiong Basin, South China: Evidence from dinosaur eggshells. Chinese Sci. Bull. 54(5),
858   806-815.

859 Zhao, Z., Yan, Z., 2000. Stable isotopic studies of dinosaur eggshells from the Nanxiong Basin,
860   South China. Sci. China Earth Sci. 43(1), 84-92.

861 Zhao, Z.K, Mao, X.Y., Chai, Z.F., Yang, G., Kong, P., Ebihara, M., Zhao, Z., 2002. A possible
862   causal relationship between extinction of dinosaurs and K/T iridium enrichment in the
863   Nanxiong Basin, South China: evidence from dinosaur eggshells. Palaeogeogr.
864   Palaeoclimatol. Palaeoecol. 178(1-2), 1-17.

865 Zhao, Z.K., Ye, J., Li, H.M., 1991. Extinction of the dinosaurs across the Cretaceous-Tertiary
866   boundary in Nanxiong Basin, Guangdong Province. Certebrata Palasiatica. 29(1), 1-20. (in
867   Chinese with English abstract)

868 Zhou, L.P., Oldfield, F., Wintle, A.G., Robinson, S.G. Wang, J., 1990. Partly pedogenic origin of
869   magnetic variations in Chinese loess. Nature. 346, 737–739.